ELSEVIER

Coordination Chemistry Reviews
216–217 (2001) 99–125

COORDINATION CHEMISTRY REVIEWS

www.elsevier.com/locate/ccr

Studies on charge distribution and valence tautomerism in transition metal complexes of catecholate and semiquinonate ligands

Cortlandt G. Pierpont *

Department of Chemistry and Biochemistry, University of Colorado, Boulder, Colorado CO 80309, USA

Received 8 August 2000; accepted 19 December 2000

Contents

Abstract

Transition metal complexes containing first row metal ions chelated by catecholate (Cat) and semiquinonate (SQ) ligands have been found to have localized electronic structures with quinone ligands bonded in both SQ and Cat electronic forms. In exceptional cases the balance of metal and quinone orbital energies is sufficiently close as to permit magnetic and spectroscopic observations on isomers differing in charge distribution together under equilibrium conditions. Equilibria occurring between $M^n(SQ^{\bullet -})$ and $M^{n+1}(Cat^{2-})$ redox isomers have been observed in solution and in the solid state for complexes of Co, Mn, and Cu. The temperature range over which equilibria may be observed, is defined by enthalpy and entropy changes associated, mainly, with changes in charge and spin-state of the metal ion. This effect has been considered as an example of valence tautomerism (VT). In this review we

* Tel.: +1-303-4926531; fax: +1-303-4920951.
E-mail address: pierpont@colorado.edu (C.G. Pierpont).

PII: S0010-8545(01)00309-5

present an overview of recent research on complexes of quinone ligands that exhibit reversible shifts in charge distribution under equilibrium conditions.

Keywords: Charge distribution; Valence tautomerism; Transition metal complexes

1. Introduction

The transition metal coordination chemistry of ligands derived from catechols and *o*-benzoquinones has been developed, primarily, over the past twenty five years with interesting and surprising results [1,2]. Initial interest in these complexes was associated with the redox activity of the quinone ligands

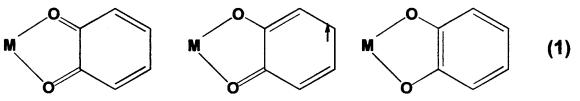

(1)

(**1**) and the potential for forming compounds that may exist in a number of electronic states due to the combined electrochemical activity of the metal ion and one or more quinone ligands [3]. The magnetic properties of complexes prepared with metals of the first transition series subsequently revealed that the partially-reduced radical semiquinone (SQ) form was stabilized upon coordination permitting observations on metal-SQ magnetic coupling, in cases where the metal ion is paramagnetic, and on metal-mediated SQ–SQ exchange for complexes containing multiple SQ ligands coordinated to a diamagnetic metal [4]. Charge delocalization within the metal–quinone chelate ring was found to be much less significant than for related complexes of the 1,2-dithiolene and diimine ligands, leading to the view that quinone-derived ligands may be described in one of the three charge–localized electronic forms shown above. Examples of all three modes of coordination are now well established [1,2].

A feature unanticipated at the outset of this research is the close separation in energy between metal and quinone electronic levels. This has led to observations on intramolecular electron transfer (ET) between redox isomers differing in charge distribution (**2**) under equilibrium conditions in a

(2)

process that we described as an example of valence tautomerism (VT) [5]. Studies on metal–quinone complexes that exhibit VT have provided fundamental insights on aspects of metal–ligand ET and stimulated interest in applications as data storage media and in sensor technology. Recent observations on a complex prepared with quinone-derived ligands indicate the potential for metal-mediated interligand electron transfer (**3**) [6].

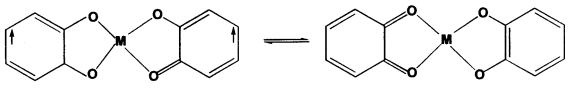

$M(SQ)_2$ (BQ)M(Cat) (3)

As the results of these studies have appeared, it has become clear that the quinone ligands will provide complexes of unique interest and versatility. We have emphasized these properties in two earlier reviews [1,2] and now describe recent results on ET and VT for quinone complexes of metals of the first transition series. Shultz has prepared a comprehensive review of VT for complexes of cobalt [7], and Dei and Gütlich have provided a brief review that describes practical applications of VT [8]. Selected aspects of quinone coordination chemistry of complexes containing second and third row metals will appear in a separate review to follow [9].

2. Quinone complexes of cobalt with initial observations on valence tautomerism

In early research we found that reactions between metal carbonyl complexes and *o*-benzoquinones provided products in a clean and simple synthetic procedure. The reaction between 3,5-di-*tert*-butyl-1,2-benzoquinone

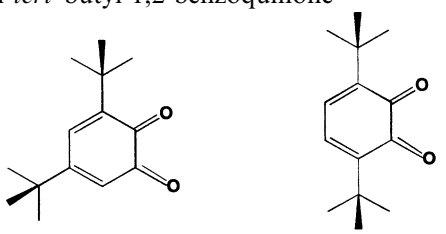

3,5-DBBQ 3,6-DBBQ

(3,5-DBBQ) and $Co_2(CO)_8$ was observed to give the $[Co^{II}(3,5\text{-DBSQ})_2]_4$ tetramer [10]. Studies on the formation of coligand addition products provided Co(bpy)(3,5-$DBQ)_2$ upon treatment with 2,2′-bipyridine [5]. Structural characterization on this complex indicated short Co–O and Co–N bond lengths, characteristic of low spin Co(III), and features for the two quinone ligands that indicated a difference in charge with one coordinated as a Cat, the second as a SQ (Fig. 1). Magnetic characterization on Co^{III}(bpy)(3,5-DBSQ)(3,5-DBCat) indicated that it had a single unpaired electron, and EPR spectra showed weak coupling to the ^{59}Co nucleus (Fig. 2), in accord with the radical–ligand/diamagnetic metal charge distribution. It was also found in solution at temperatures near room temperature, that the EPR spectrum disappeared as the paramagnetically shifted ^1H-NMR spectrum of a Co(II) species appeared. Electronic spectra recorded in solution over the temperature range at which changes in the NMR and EPR spectra were observed to occur (Fig. 3) showed that the Co(III) and Co(II) redox isomers of the complex were together in thermal equilibrium [11]. Variable temperature magnetic measurements recorded on both solution and solid samples (Fig. 4) supported the spectral observations pointing to an equilibrium between species related by metal–quinone

electron transfer with an associated change in spin multiplicity for the metal [12]. The critical temperature (Tc) for the equilibrium, defined as the temperature at which Co(III) and Co(II) redox isomers are present at equal concentration, was obtained from both solid state magnetic measurements and spectral changes in solution. Solution measurements indicated that the critical temperature was solvent dependent with Tc shifted to higher temperatures with an increase in solvent polarity. Thermodynamic parameters obtained from measurements made on changes in magnetism in the solid state and from spectral changes in toluene solution indicated that values for both the enthalpy and entropy change were relatively large and positive in sign [13]. The enthalpy change is associated, primarily, with weakened Co–O and Co–N bonds as the result of electrons entering the dσ antibonding e_g orbital of the metal with the change in electronic structure from ls-Co(III) to hs-Co(II) (Fig. 5). The increase in density of vibrational states resulting from weakened bonds and increased conformational flexibility for the complex in solution contribute to a large positive entropy change. Together, the values for $\Delta H°$ and $\Delta S°$ define Tc [13].

Subsequent research has been directed at studies with different nitrogen donor ancillary ligands and on complexes prepared with quinone ligands derived from symmetrical 3,6-DBBQ [12]. As a general result, strong N-donor ligands increase Tc. This has been illustrated by the effect of adding alkyl and nitro substituents to bpy and phen as shown in Table 1. Alkyl groups increase Tc over the values

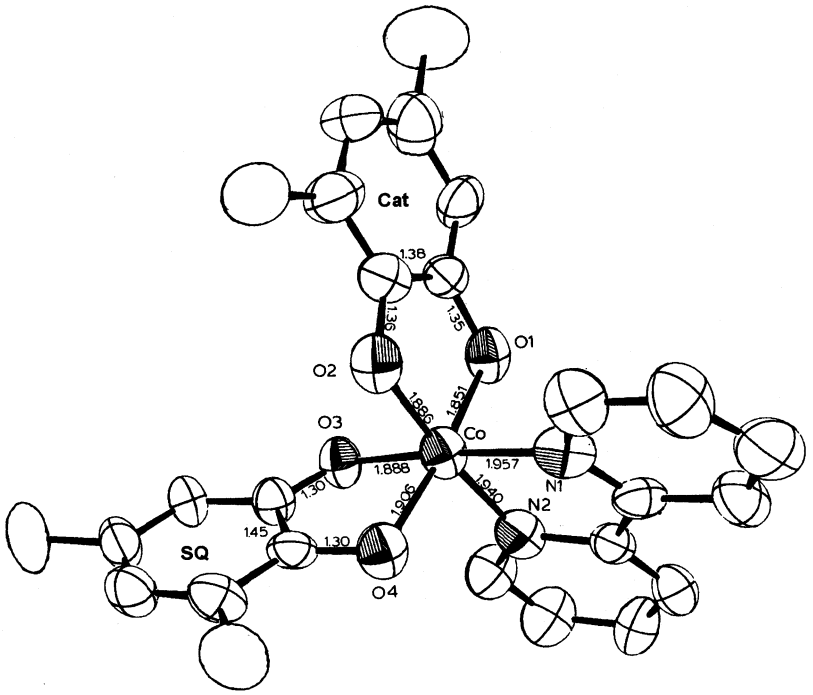

Fig. 1. View of Co^{III}(bpy)(3,5-DBSQ)(3,5-DBCat) with *tert*-butyl methyl carbon atoms omitted.

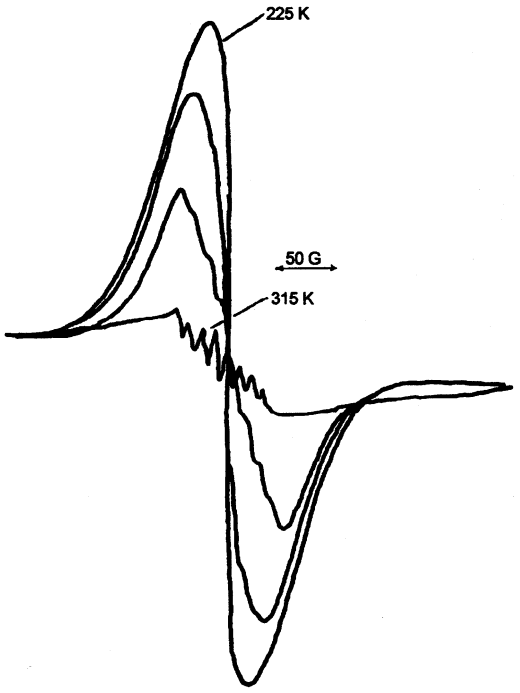

Fig. 2. Temperature-dependent changes in the EPR spectrum of Co^{III}(bpy)(3,5-DBSQ)(3,5-DBCat) in toluene solution.

obtained for complexes prepared with the unsubstituted coligands [14]. Nitro groups decrease Tc so that the Co(II) redox isomer, Co^{II}(N-N)(3,6-DBSQ)$_2$ is obtained by crystallization at room temperature (Fig. 6). Structural characterization has indicated that these molecules have trigonal prismatic (TP) coordination geometries, and ligand field effects block the shift in charge distribution to the Co(III) isomer. The complexes observed to have TP structures are locked into the Co(II) charge distribution in the solid state [12].

The effect of chelate ring flexibility, and the associated increase in $\Delta S°$, appears dramatically for Co(tmeda)(3,6-DBSQ)(3,6-DBCat) (Tc = 310 K) (Fig. 7) and Co(tmpda)(3,6-DBSQ)$_2$ (Tc = 110 K) with the addition of one methylene carbon to the chelate ring (Table 2).[15] *Cis*/*trans* changes in octahedral coordination geometry appear to not be a significant effect. Measurements on *trans*-Co(py)$_2$(3,6-DBSQ)(3,6-DBCat) appear similar to Co(bpy)(3,6-DBSQ)(3,6-DBCat) [16].

Light-induced shifts in charge distribution have been investigated with the result that Co(III) redox isomers have been observed to convert to the Co(II) form upon irradiation. Electronic spectra recorded on Co^{III}(N-N)(DBSQ)(DBCat) complexes show prominent transitions in the 600 and 2500 nm regions (Fig. 8). SCF calculations assign the 600 nm transition as π–π^* with considerable MLCT character from the composition of the orbitals of Co(phen)(SQ)(Cat) [17]. The transition at 2500 nm is an IT transition between the mixed-charge Cat and SQ

ligands. We had earlier suggested that this might be a low energy Cat → Co(III) charge transfer transition based on several observations [12]. Related mixed charge ligand complexes of Fe(III), Cr(III), and Ga(III) failed to show bands in this region and they fail to undergo VT. Irradiation on Co(N-N)(SQ)(Cat) complexes with light from a tungsten lamp was observed to result in a shift to the Co(II) redox isomer. These observations were made in experiments of two types. 'Crystal bending' experiments were carried out on thin crystals of the supported pyrazine-bridged polymer $[Co^{III}(\mu\text{-pyz})(3,6\text{-DBSQ})(3,6\text{-DBCat})]_n$ (Fig. 9) and on Co^{III}(bpy)(3,6-DBSQ)(3,6-DBCat) (Fig. 10) [18,19]. The crystal structure of the bpy complex consists of linear arrays of complex molecules linked by bpy stacking interactions, and both crystal structures consist of a complex core within a hydrocarbon sheath formed by the ring and *tert*-butyl groups of the quinone ligands. All crystals that have been observed to show photomechanical properties have this structural feature, contributing to a 'soft' solid state environment for the

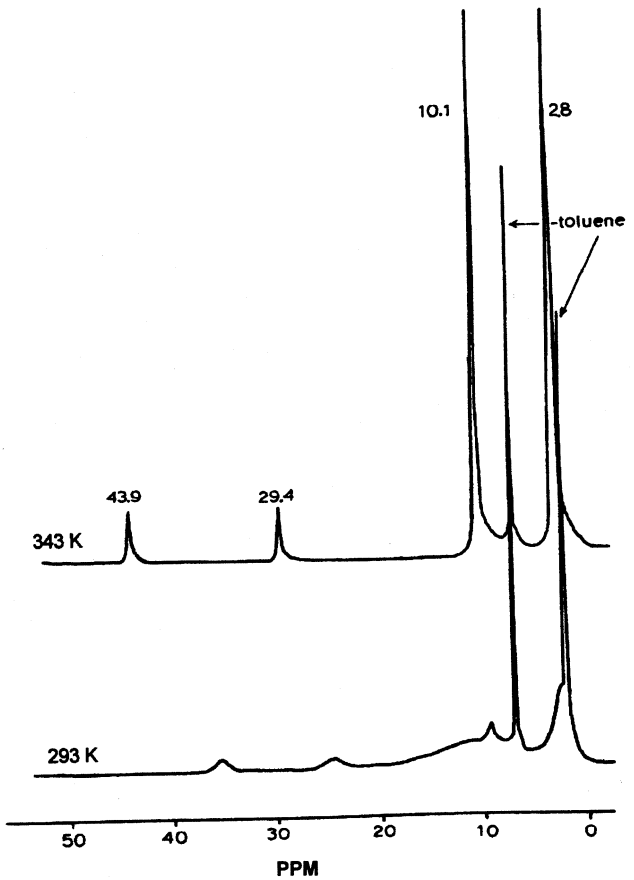

Fig. 3. The appearance of a paramagnetically shifted ^{1}H-NMR spectrum with the formation of Co^{II}(bpy)(3,5-DBSQ)$_2$.

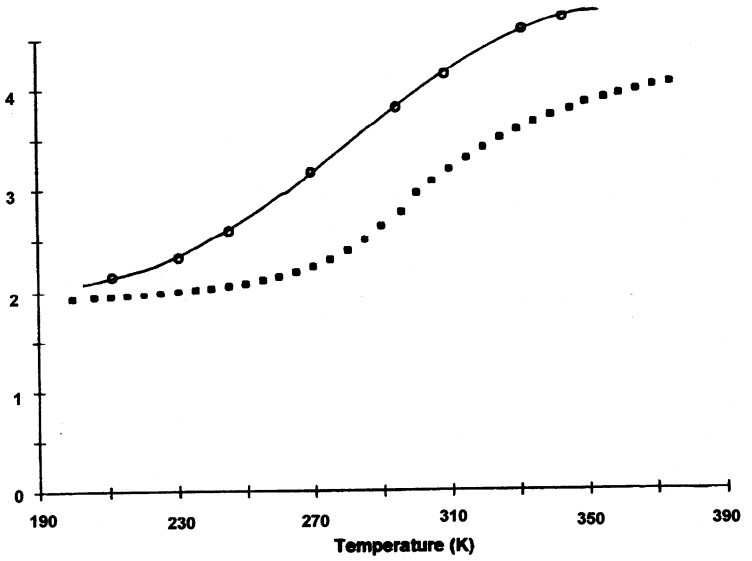

Fig. 4. Changes in magnetic moment with the shift from Co^{III}(bpy)(3,5-DBSQ)(3,5-DBCat) to Co^{II}(bpy)(3,5-DBSQ)$_2$ in toluene solution (○) and in the solid state (■).

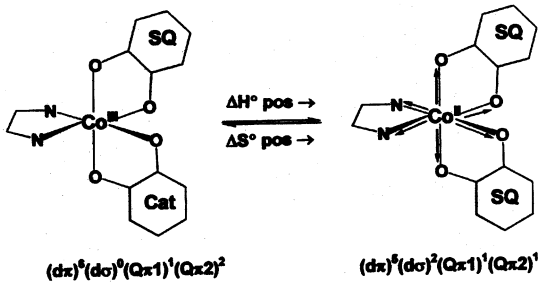

Fig. 5. Changes in the inner coordination sphere with charge and the spin-state for Co.

complex polymer, and with intense transitions at low energy [20]. In the case of the pyrazine and bipyridine complexes of Co, the effect appears to result from the change in radius of the metal with the transition from ls-Co(III) to hs-Co(II) propagated along the axis of the polymer [18]. As a LL′IT transition the absorption at 2500 nm provides a broad absorption cross section for energy transfer to the complex in a process that does not directly involve optical electron transfer.

In a second series of experiments light induced shifts in charge distribution were investigated for the Co complex prepared with the bipyridine ether (py_2O) coligand [21]. Crystals of this complex obtained at room temperature by crystallization from toluene were found to contain the $Co^{II}(py_2O)(3,6\text{-DBSQ})_2$ redox isomer (Fig. 11); crystals obtained by crystallization from acetone contained $Co^{III}(py_2O)$(3,6-DBSQ)(3,6-DBCat) (Fig. 12). The py_2O ligand of the $Co^{II}(py_2O)(3,6\text{-DBSQ})_2$

isomer is planar and the solid state lattice consists of stacked complex molecules linked by pairing interactions between py_2O ligands. The $Co^{III}(py_2O)$(3,6-DBSQ)(3,6-DBCat) lattice consists of well-separated molecules with a folded structure for the py_2O ligands that presumably results from constraints associated with the smaller radius of the Co(III) ion. The stacked lattice of $Co^{II}(py_2O)$(3,6-DBSQ)$_2$ prevents folding of the py_2O ligand, and measurements show a magnetic moment that is constant at the value of the Co(II) isomer down to 25 K. In contrast, freshly prepared crystalline samples of the Co(III) isomer show hysteresis of nearly 200°

Table 1
Influence of N-N coligand on *T*c for complexes of the Co(N-N)(3,6-DBQ)$_2$ series in toluene solution

N-N	*T*c (K)	Reference
Ph_2bpy [a]	350	[14]
tmeda	310	[15]
Me_2bpy [a]	287	[14]
tmmda	280	[15]
bpy	275	[12]
phen	265	[12]
tmpda	<180 [b]	[15]
NO_2-phen	<180 [b]	[12]
$(NO_2)_2$-bpy	<180 [b]	[c]

[a] Values obtained for complexes prepared with the 3,5-DBQquinone ligand.
[b] *T*c occurs below the freezing point of toluene.
[c] O.-S. Jung, personal communication.

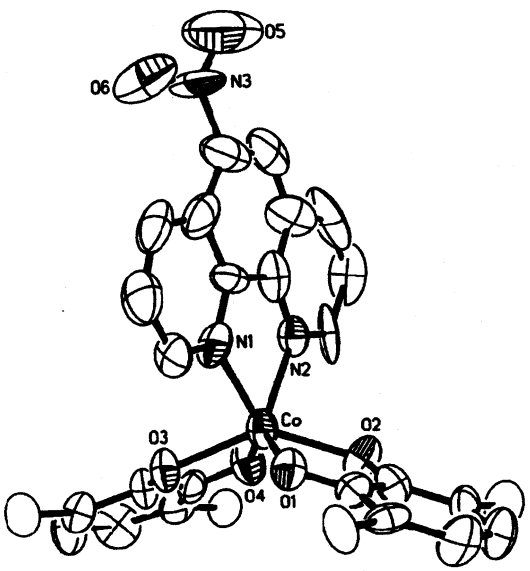

Fig. 6. View of trigonal prismatic $Co^{II}(NO_2$-phen)(3,6-DBSQ)$_2$.

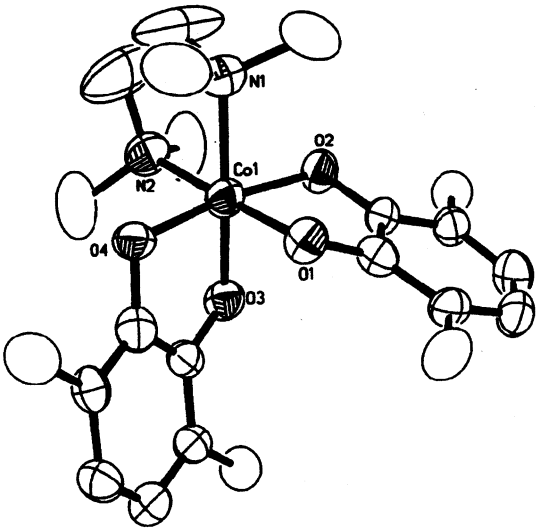

Fig. 7. View of Co^{III}(tmeda)(3,6-DBSQ)(3,6-DBCat).

Table 2
Structural parameters and solid state *T*c values for members of the $Co(Me_2N(CH_2)_nNMe_2)(3,6\text{-}DBQ)_2$ series

	TMMDA	TMEDA	TMPDA
Co-O (Å)	1.868(3)	1.872(2)	2.019(4)
Co-N (Å)	1.998(3)	2.026(2)	2.181(4)
N–Co–N (°)	71.8(1)	87.1(1)	94.5(2)
*T*c (solid) (K)	375	350	178

between Co(III) → Co(II) and Co(II) → Co(III) steps (Fig. 13).[21] Repeated traces show a gradual breakdown in hysteresis indicating that the Co(III) isomer is metastable at temperatures above 250 K. Irradiation of a sample of the Co(III) isomer in the form of a KBr pellet at 270 K with a tungsten lamp was observed to result in an irreversible shift to the Co(II) isomer as observed from changes in the optical spectrum. It has been of interest to see if irradiation at the 770 nm transition of the $Co^{II}(py_2O)(3,6\text{-}DBSQ)_2$ isomer, a MLCT band, at a temperature where this isomer is metastable (~ 200 K), produces $Co^{III}(py_2O)$(3,6-DBSQ)(3,6-DBCat). To date we have not observed light-induced switching from Co(II) to Co(III), but it occurs thermally in the cycle of magnetic changes of $Co(py_2O)(3,6\text{-}DBQ)_2$.

Hendrickson has studied the electrochemical properties of $Co(bpy)(3,5\text{-}DBQ)_2$ with striking results [22]. Reduction of the complex either chemically or electro-

chemically at different temperatures was found to result in products that reflect the presence of different redox isomers in solution. Cobaltocene reduction of Co^{III}(bpy)(3,5-DBSQ)(3,5-DBCat) at lower temperature (CH_2Cl_2, 273 K) gives dark green $(CoCp_2)[Co^{III}(bpy)(3,5\text{-}DBCat)_2]$: reduction at

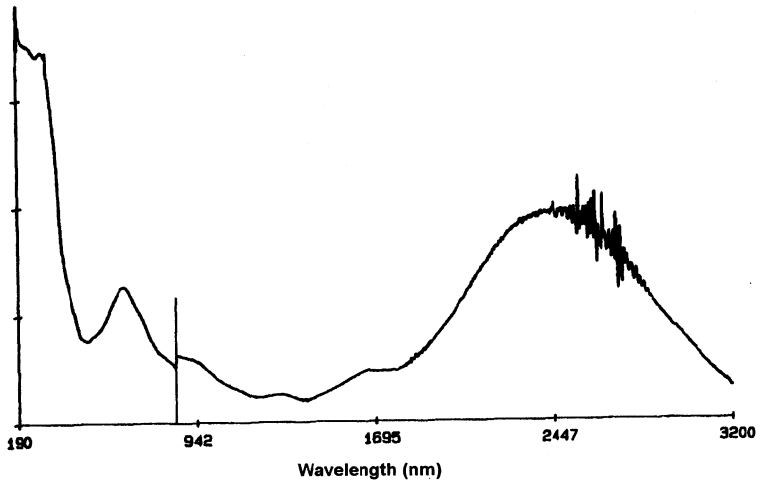

Fig. 8. Electronic spectrum of Co^{III}(tmeda)(3,6-DBSQ)(3,6-DBCat) recorded as a solid KBr pellet at 295 K.

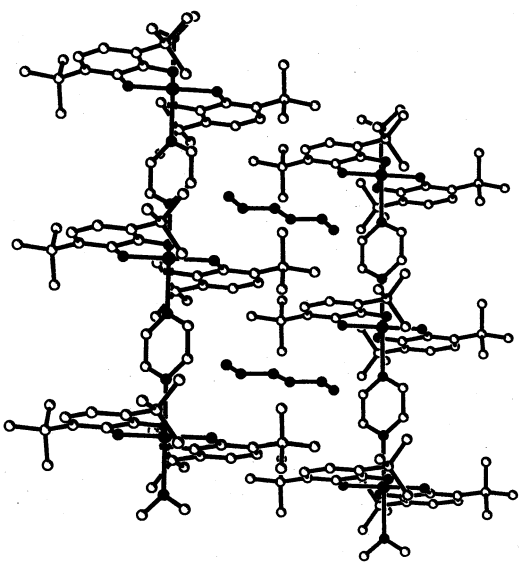

Fig. 9. View of the $[Co^{III}(\mu\text{-pyz})(3,6\text{-}DBSQ)(3,6\text{-}DBCat)]_n$ polymer obtained as the hexane solvate.

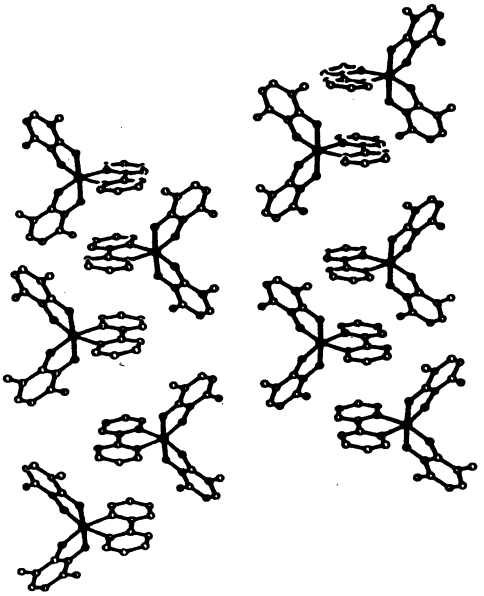

Fig. 10. Stacked solid state structure of Co^{III}(bpy)(3,6-DBSQ)(3,6-DBCat).

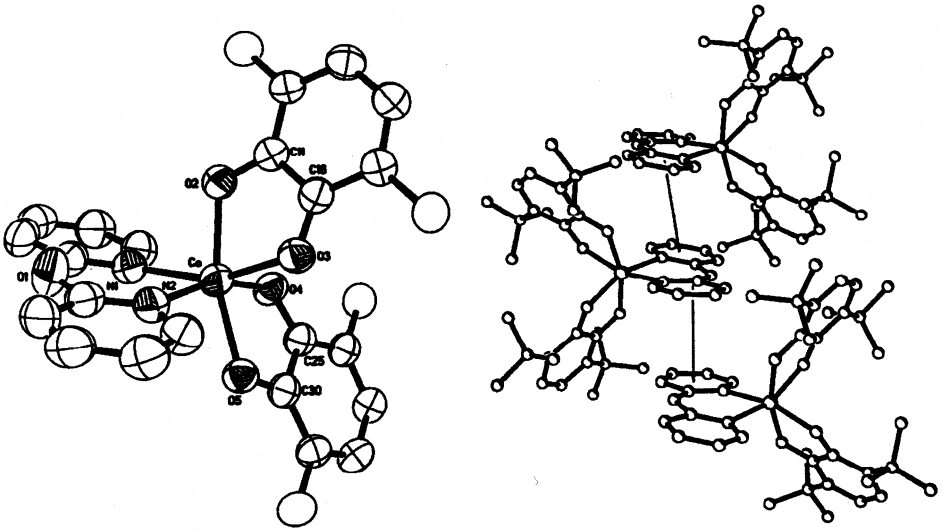

Fig. 11. Molecular and crystal structures of $Co^{II}(py_2O)(3,6\text{-}DBSQ)_2$.

$$Co^{III}(bpy)(3,5\text{-DBSQ})(3,5\text{-DBCat}) + CoCp_2 \rightarrow$$
$$(CoCp_2)[Co^{III}(bpy)(3,5\text{-DBCat})_2]$$

a higher solution temperature (toluene, 345 K) gave

$$Co^{II}(bpy)(3,5\text{-DBSQ})_2 + CoCp_2 \rightarrow$$
$$(CoCp_2)[Co^{II}(bpy)(3,5\text{-DBSQ})(3,5\text{-DBCat})]$$

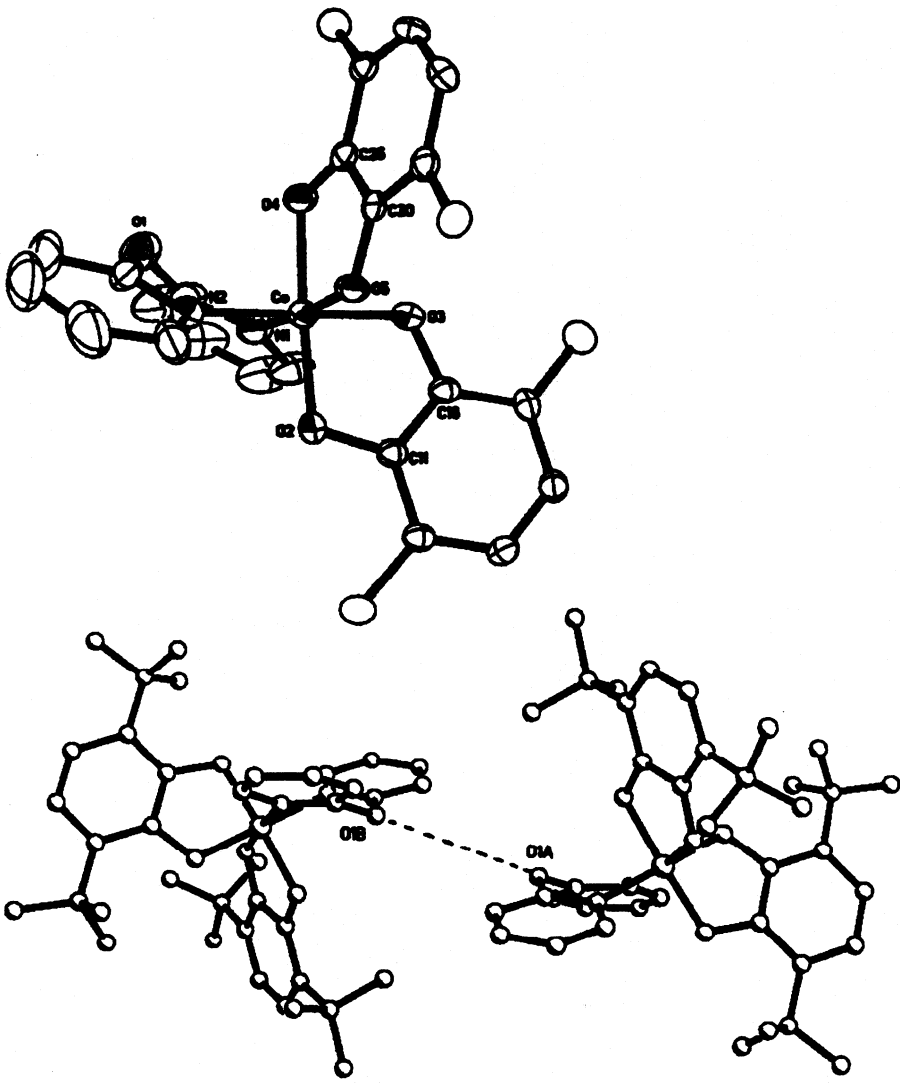

Fig. 12. Molecular and crystal structures of $Co^{III}(py_2O)(3,6\text{-DBSQ})(3,6\text{-DBCat})$ showing the folded py_2O ligand.

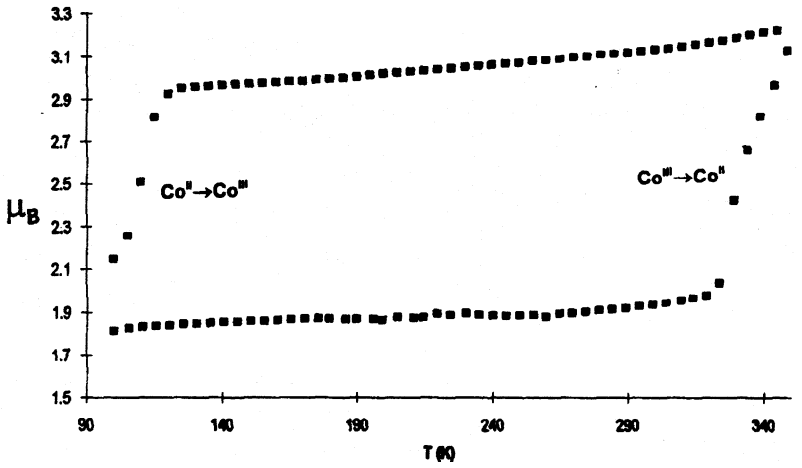

Fig. 13. Magnetic hysteresis in shifts between $S = 1/2Co^{III}(py_2O)(3,6\text{-DBSQ})(3,6\text{-DBCat})$ and high-spin $Co^{II}(py_2O)(3,6\text{-DBSQ})_2$ redox isomers in the solid state.

$(CoCp_2)[Co^{II}(bpy)(3,5\text{-DBSQ})(3,5\text{-DBCat})]$. In both cases reduction occurs at a SQ ligand of the redox isomer, rather than at the metal. Further, the redox isomers formed upon reduction were observed to exhibit valence tautomerism. This has formed the basis for the cyclic array of redox isomers and reduction products related by intra- and intermolecular ET steps shown in Fig. 14 [22].

Observations on valence tautomerism for the quinone complexes of cobalt are centered about thermodynamic changes that result from the transfer of charge to and from antibonding orbitals directed at ligands, the dσ e_g orbitals of the octahedral complex (Fig. 5). *Tert*-butyl substituents of the ligands encapsulate the complex, reducing, but not eliminating, solvent effects. All complexes that have been reported to exhibit VT have been prepared with either 3,5- or 3,6-di-*tert*-butyl-catecholate or semiquinonate ligands. Dei has observed VT for a ligand obtained by Schiff base condensation of two 3,5-DBCat ligands with ammonia [23]. When carried out in the presence of $CoCl_2$ the complex shown in Fig. 15 was obtained [24]. As with the quinones, the tridentate ligand resulting from condensation may exist in several charged forms. The two forms that appear most commonly in the coordination chemistry are the Cat-N-BQ

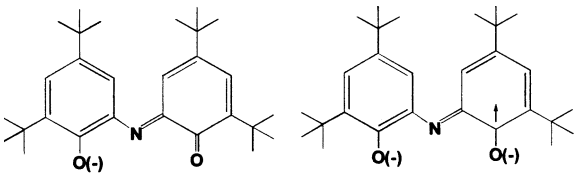

anion and the Cat-N-SQ radical dianion. Structural, spectral, electrochemical, and magnetic properties of this complex indicated the Co(III) redox isomer with mixed

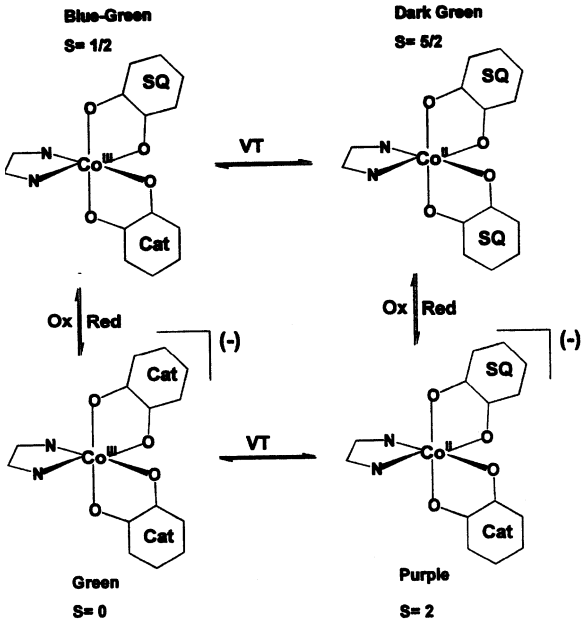

Fig. 14. Cycle of VT equilibria and redox steps for redox isomers of Co(bpy)(3,5-DBQ)$_2$ and [Co(bpy)(3,5-DBQ)$_2$]$^-$.

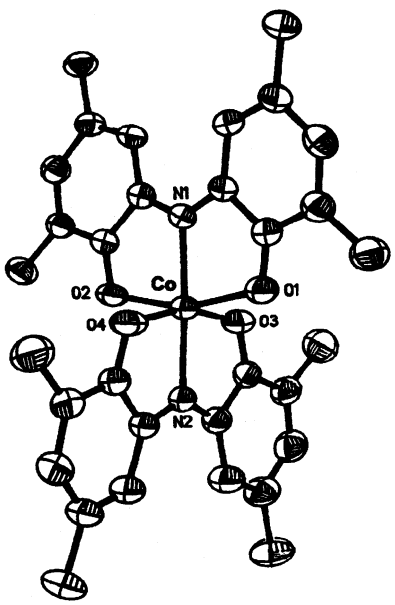

Fig. 15. View of the Co^{III}(Cat-N-BQ)(Cat-N-SQ) redox isomer at 295 K.

charge ligands Co(Cat-N-BQ)(Cat-N-SQ) [24]. Dei has reported spectral changes in toluene solution over the temperature range between 295 and 360 K that have been interpreted as indicating an equilibrium between Co(III) and Co(II) redox isomers in an equilibrium that is similar to the equilibria of the Co(N-N)(SQ)(Cat) series [23]. Further, Chaudhuri and Wieghardt have recently observed intramolecular interligand electron transfer for $Zn(Cat–N–BQ)_2$ [6]. This ligand appears to offer great potential for studies on intramolecular ET. However, these studies should be made with care; it has been shown that intramolecular cyclization may occur to give the interesting phenoxazinylate radical that may also participate in ET reactions as an iminoquinone ligand [25].

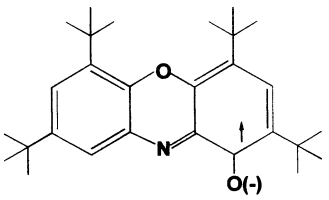

3. Quinone complexes of Mn and the potential for bimodal valence tautomerism

The model for VT that associates temperature-dependent equilibria between redox isomers with differences in population of the octahedral antibonding e_g dσ level should apply to metal ions other than the hs-Co(II) | ls-Co(III) couple. Manganese commonly forms complexes as hs-d^5 Mn(II) and hs-d^4 Mn(III), and less commonly as d^3 Mn(IV). This series has the requisite changes in dσ population, but without the spin transition of cobalt. Consequently, the quinone complexes of manganese have been of interest in the extension of VT to compounds containing other metal ions. Crystallographic studies on complexes of manganese show the changes in bonding for each of the metal ions that would lead to changes in energy favorable for VT. Octahedral d^3

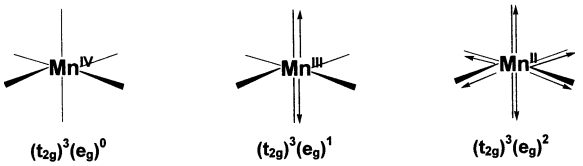

Mn(IV) with high positive charge and an unpopulated dσ level forms strong bonds with O- and N-donor ligands. This high oxidation state is generally observed for complexes containing O-donor ligands that provide charge to the metal through strong π-donation. Alkoxo and catecholate ligands are strong π donors, and $[Mn^{IV}(3,5\text{-DBCat})_3]^{2-}$ was one of the early examples of Mn(IV) coordination [26]. It resembles ls-Co(III) in forming complexes with strong ligand bonds, and with a rigidly octahedral geometry. In its coordination properties Mn(II) is the antithesis of Mn(IV). It is generally high-spin with a $t_{2g}^3 e_g^2$ configuration. Two electrons are

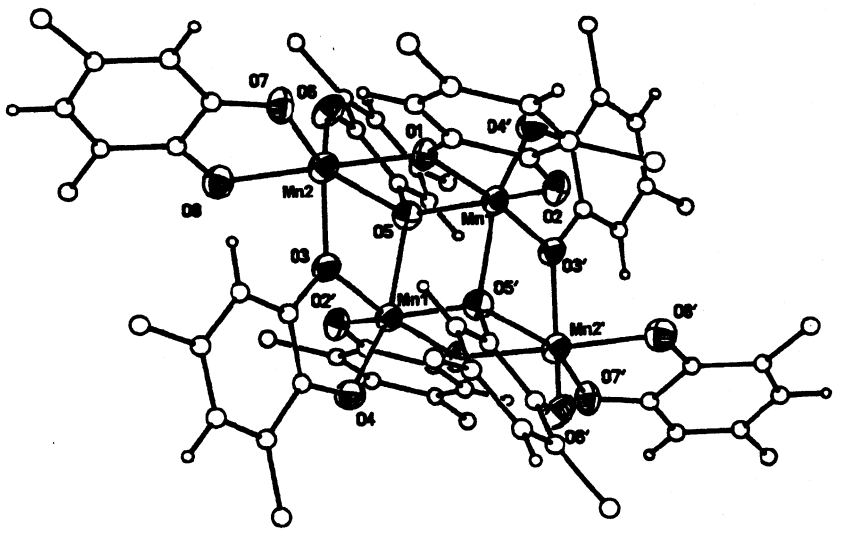

Fig. 16. View of the $[Mn^{II}(3,5\text{-}DBSQ)_2]_4$ tetramer. Related complexes of Co(II) and Ni(II), and $Fe_4^{III}(3,5\text{-}DBSQ)_4(3,5\text{-}DBCat)_4$ have similar structures.

directed at ligand bonding sites similar to hs-Co(II), and the Mn(II) ion has a flexible coordination geometry. The reaction between $Mn_2(CO)_{10}$ and 3,5-DBBQ was found to give the $[Mn^{II}(3,5\text{-}DBSQ)_2]_4$ tetramer [27], with a structure very similar to that of the related Co tetramer (Fig. 16) [10]. Similarities between Mn(IV) with Co(III) and Mn(II) with Co(II) are clear; the obvious difference is the intermediate oxidation state of manganese, Mn(III). But, even this ion with its $t_{2g}^3e_g^1$ configuration resembles the ls-Co(II) ion ($t_{2g}^3e_g^1$) that is formed upon ET to ls-Co(III) prior to spin transition as a short-lived intermediate.

The addition of pyridine to $[Mn^{II}(3,5\text{-}DBSQ)_2]_4$ was found to give *trans*-$Mn^{IV}(py)_2(3,5\text{-}DBCat)_2$ [28], and related reactions carried out with 3,6-DBBQ have been used to form $Mn^{IV}(2,2'\text{-}bpy)(3,6\text{-}DBCat)_2$ and *trans*-$Mn^{IV}(Bu\text{-}py)_2(3,6\text{-}DBCat)_2$ (Fig. 17) [16,29]. For bond lengths to the Mn centers, all three molecules are short and are values expected for Mn(IV) (Table 3). Studies on polymeric complexes have produced the pyrazine-bridged polymer $[Mn^{III}(\mu\text{-}pyz)(3,6\text{-}DBSQ)(3,6\text{-}DBCat)]_n$ (Fig. 18), the *trans*-$Mn^{III}(4,4'\text{-}bpy)_2(3,6\text{-}DBSQ)(3,6\text{-}DBCat)$ monomer, and *trans*-$Mn^{III}(thf)_2(3,6\text{-}DBSQ)(3,6\text{-}DBCat)$ as a potential polymer precursor [29–31]. Bond lengths to the metals in each case show axial lengthening as a signature of the tetragonally distorted Mn(III) ion. As with the complexes of Co, weak N-donor ligands lead to Mn(II). This was found for $[Mn^{II}(3,5\text{-}DBSQ)_2]_4$ where weak bridging interactions from SQ oxygens link adjacent Mn(II) centers that are nearly five-coordinate [27], and for $Mn^{II}(NO_2\text{-}phen)(3,6\text{-}DBSQ)_2$ with long Mn–O and Mn–N lengths and a trigonal prismatic coordination geometry [29]. With this series of complex coligand-dependent shifts, Mn-quinone charge distribution have been defined, pointing to the existence of three stable redox isomers.

Mn^{IV}(N-N)$(DBCat)_2$	Mn^{III}(N-N)(DBSQ)(DBCat)	Mn^{II}(N′N)$(DBSQ)_2$
$(d\pi)^3(d\sigma)^0(Q\pi1)^2(Q\pi2)^2$	$(d\pi)^3(d\sigma)^1(Q\pi1)^1\ (Q\pi2)^2$	$(dp)^3(ds)^2(Qp1)^1(Qp2)^1$

Observations on VT for the complexes of Mn have been made from changes in electronic spectrum in solution and in the solid state. Changes in magnetism that occur with shifts in charge distribution have not been of use in the Mn series because the $Mn^{IV}(Cat)_2$, $Mn^{III}(SQ)(Cat)$, and $Mn^{II}(SQ)_2$ redox isomers all have $S = 3/2$ spin ground states due to antiferromagnetic Mn-SQ coupling [29]. Observations on changes in optical spectra are complicated by the appearance of a strong Cat → Mn LMCT band at 880 nm that results in spectral similarity in the visible

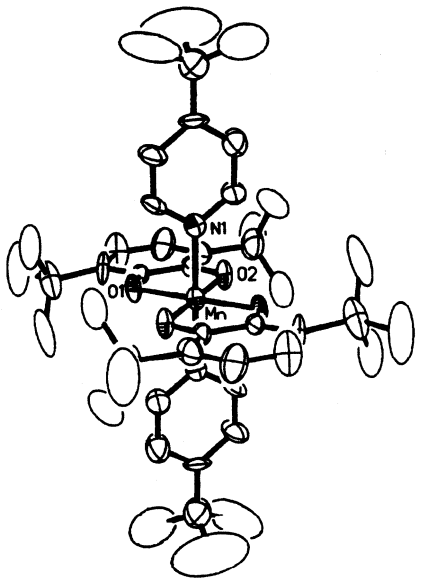

Fig. 17. View of *trans*-Mn^{IV}(*tert*-Bupy)$_2$(3,6-DBCat)$_2$.

Table 3
Bond lengths for redox isomers of the Mn(N-N)(3,6-DBQ)$_2$ series

	Mn–O (Å)	Mn–N (Å)
Mn(IV)		
$Mn(py)_2$(3,5-DBCat)$_2$	1.853	2.018
$Mn(Bupy)_2$(3,6-DBCat)$_2$	1.853	2.034
Mn(2,2'-bpy)(3,6-DBCat)$_2$	1.866	2.086
Mn(III)		
$Mn(4,4'\text{-bpy})_2$(3,6-DBSQ)(3,6-DBCat)	1.886	2.273
$[Mn(\mu\text{-pyz})(3,6\text{-DBSQ})(3,6\text{-DBCat})]_n$	1.854	2.375
Mn(II)		
$Mn(NO_2\text{-phen})(3,6\text{-DBSQ})_2$	2.148	2.296

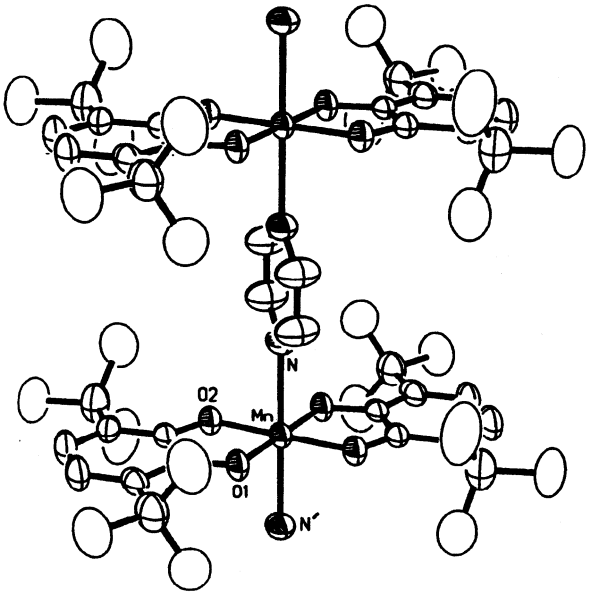

Fig. 18. View of one unit of the [*trans*-Mn^{III}(μ-pyz)(3,6-DBSQ)(3,6-DBCat)]$_n$ polymer.

region for the $Mn^{IV}(Cat)_2$ and $Mn^{III}(SQ)(Cat)$ redox isomers. Changes in the intensity of a low-energy LL′CT transition between Cat and SQ ligands of the $Mn^{III}(SQ)(Cat)$ isomer in the 2000–2200 nm region have permitted observations on VT in the solid state. Electronic spectra of the $Mn^{II}(SQ)_2$ redox isomers consist of relatively weak transitions at 420 and 750 nm. Observations on the shift from the Mn(III) isomer to Mn(II) are best observed in the solid state as a decrease in intensity in the 2100 nm region with increasing temperature, and the shift from Mn(IV) to Mn(III) as an intensity increase in this region [29,31].

Initial observations on VT for the Mn complexes came from the solution behavior of $Mn^{IV}(py)_2$(3,5-DBCat)$_2$ [28]. Reversible changes in color, from the intense red–purple of $Mn^{IV}(py)_2$(3,5-DBCat)$_2$ and $Mn^{III}(py)_2$(3,5-DBSQ)(3,5-DBCat) to the pale green–brown of $Mn^{II}(py)_2$(3,5-DBSQ)$_2$ pointed to an equilibrium similar to that of Co(bpy)(3,5-DBSQ)(3,5-DBCat). In subsequent studies, solid state spectra recorded on *trans*-$Mn^{IV}(Bu\text{-}py)_2$(3,6-DBCat)$_2$ at the temperature used for crystallographic characterization showed the expected transitions at 520 and 880 nm for the Mn(IV) redox isomer, but a weak transition at 2123 nm. The intensity of this low energy transition was observed to increase reversibly with increasing temperature with the shift to the Mn(III) isomer. Similar observations have been made for Mn^{IV}(2,2′-bpy)(3,6-DBCat)$_2$ in the solid state indicating a shift to Mn^{III}(2,2′-bpy)(3,6-DBSQ)(3,6-DBCat)$_2$ (Fig. 19). In toluene solution at room temperature both complexes give spectra of the Mn(II) isomer and show a return to the intense red–purple color of Mn(III) upon cooling in liquid N_2.

Observations on shifts from the Mn(III) to the Mn(II) redox isomer in the solid state have been made for both Mn^{III}(4,4′–bpy)$_2$(3,6-DBSQ)(3,6-DBCat) and the

$[Mn^{III}(\mu\text{-pyz})(3,6\text{-DBSQ})(3,6\text{-DBCat})]_n$ polymer (Fig. 20) [29,30]. Intense Cat → SQ transitions appear at 2170 and 2090 nm, respectively, for the compounds in the solid state. The intensities of both transitions were observed to decrease with increasing temperature, as would accompany the shift to the Mn(II) isomer. Magnetic measurements recorded on samples of all three redox isomers show a slight temperature dependence with magnetic moment dropping from a value near

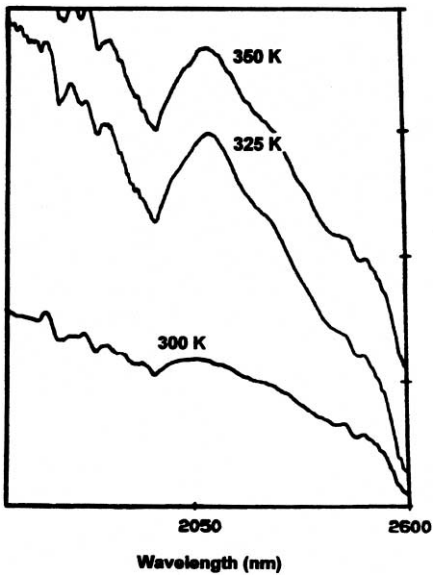

Fig. 19. Spectral changes in the 2100 nm region of $Mn^{IV}(2,2'\text{-bpy})(3,6\text{-DBCat})_2$ in the solid state that show the shift to the $Mn^{III}(2,2'\text{-bpy})(3,6\text{-DBSQ})(3,6\text{-DBCat})$ redox isomer with increasing temperature.

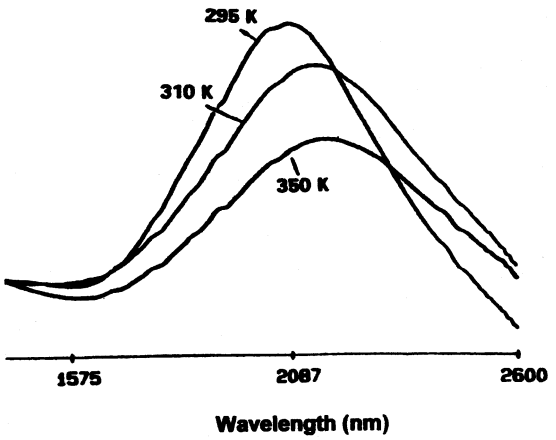

Fig. 20. Temperature-dependent spectral changes in the 2100 nm region of $[trans\text{-}Mn^{III}(\mu\text{-pyz})(3,6\text{-DBSQ})(3,6\text{-DBCat})]_n$ that show the shift to the Mn(II) redox isomer.

4.0μ_B at temperatures near room temperature to approximately 3.7μ_B at 25 K. In no case was there an abrupt change in magnetic moment associated with an isomeric shift as for the Co complexes.

Spectral changes that occur in solution and in the solid state for the Mn quinone complexes indicate a two-step shift in charge distribution that follows the pattern of effects of weakened M–L bonds with population of the dσ orbital proposed to account for observations on the Co series. An important difference with Mn lies in the relative stability of the Mn(III) redox isomer compared with the ls-Co(II) isomer that rapidly undergoes spin transition to hs-Co(II). Otherwise, Co equilibria would occur in separate observable ET and ST steps.

As with Co, it has been of interest to extend observations on VT to complexes other than members of the $Mn(N\text{-}N)(DBQ)_2$ series. Dei has reported that $[Mn(CTH)(3,5\text{-}DBQ)]^+$ may be isolated in the solid state in the form of green $[Mn^{III}(CTH)(3,5\text{-}DBCat)]^+$ and yellow $[Mn^{II}(CTH)(3,5\text{-}DBSQ)]^+$ redox isomers [32]. Thermal equilibria were observed for the compound in the solid state and in solution. We have reported that while the reaction between $Mn_2(CO)_{10}$ and 3,5-DBBQ gives the $[Mn^{II}(3,5\text{-}DBSQ)_2]_4$ tetramer, reactions carried out with 3,6-DBBQ give $Mn(3,6\text{-}DBQ)_3$ [31]. Structural and spectral characterization on the complex in the solid state at room temperature are consistent with a $Mn^{IV}(3,6\text{-}DBSQ)_2(3,6\text{-}DBCat)$ charge distribution (Fig. 21). The complex exhibits an intense transition at 2300 nm in accord with the mixed-charge ligand formulation. Spectral changes that occur in the solid state with increasing temperature were interpreted as indicating a shift to the $Mn^{III}(3,6\text{-}DBSQ)_3$ redox isomer. Changes in intensity of the 2300 nm transition with the shift to the Mn(III) isomer are shown in Fig. 22.

Observations on complexes of Mn with one, two or three quinone ligands show that the effects responsible for VT in the quinone complexes of Co may be extended to complexes of other metals. It has been of interest to investigate the related complexes of iron as the metal that lies between Mn and Co in the first transition series. Characterization on the series of complexes of general form $Fe^{III}(N\text{-}N)(SQ)(Cat)$, where both 3,5- and 3,6-DBBQ have been used and for a variety of N-donor coligands, has failed to indicate a shift in oxidation state for the metal [33]. With this, $Fe^{III}(bpy)(3,6\text{-}DBSQ)(3,6\text{-}DBCat)$ was observed to show a marked drop in magnetic moment with temperature and unusually large solvatochromic shifts in electronic spectra. Nevertheless, Mössbauer spectra have failed to detect a change in charge or spin-state for the metal in the solid state. This observation is reasonable when viewed in the context of the energy changes responsible for VT with Co and Mn. The Cat complexes of iron commonly contain hs-$Fe^{III}(Cat)$ species and ET to the metal would likely result in a hs-$Fe^{II}(SQ)$ redox isomer. In the absence of a change in the population of the dσ orbital there are no thermodynamic changes favoring a temperature-dependent shift in charge distribution.

$$Fe^{III}(N\text{-}N)(DBSQ)(DBCat) \qquad Fe^{II}(N\text{-}N)(DBSQ)_2$$
$$(d\pi)^3(d\sigma)^2(Q\pi 1)^1\ (Q\pi 2)^2 \qquad (d\pi)^4(d\sigma)^2(Q\pi 1)^1\ (Q\pi 2)^1$$

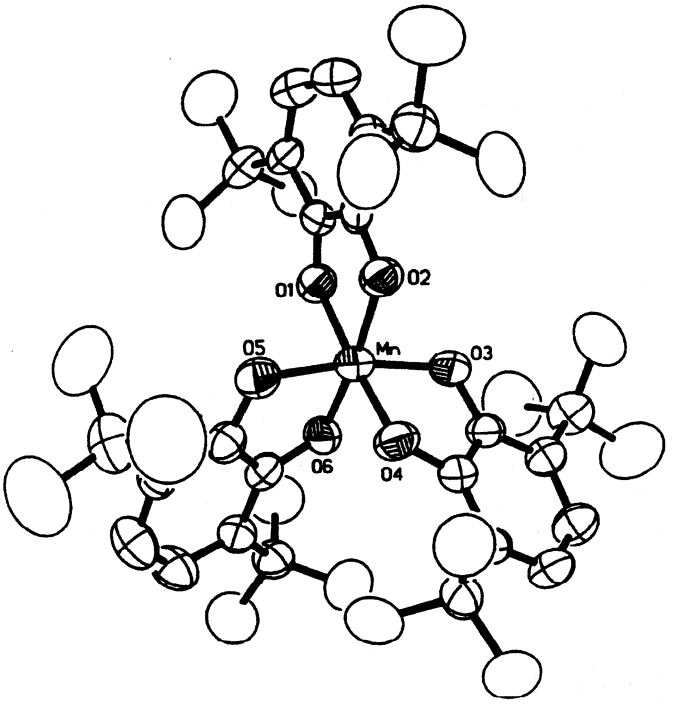

Fig. 21. View of $Mn^{IV}(3,6\text{-DBSQ})_2(3,6\text{-DBCat})$.

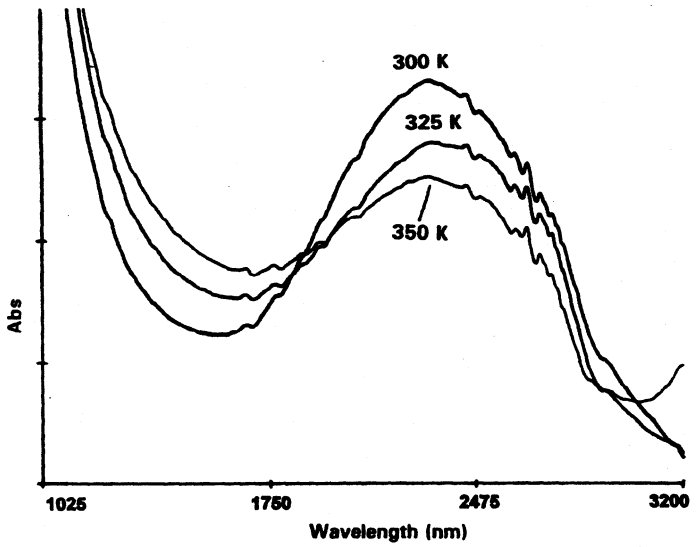

Fig. 22. Temperature-dependent spectral changes in the 2300 nm region for $Mn^{IV}(3,6\text{-DBSQ})_2(3,6\text{-DB-Cat})$ that show the shift to $Mn^{III}(3,6\text{-DBSQ})_3$ with increasing temperature in the solid state.

4. Valence tautomerism for quinone complexes of copper

Quinone complexes of copper may exist in the form of two isoelectronic redox isomers, L_nCu^{II}(Cat) and L_nCu^{I}(SQ) [34]. Charge distribution is defined by the donor properties of the ancillary ligands. Phosphine ligands result in a Cu^{I}(SQ) charge distribution with a tetrahedral coordination geometry and a complicated radical EPR spectrum containing hyperfine coupling with the ^{31}P, $^{63,65}Cu$, and semiquinone ring protons (Fig. 23). Hard nitrogen donor ligands increase valence orbital energy of the metal resulting in a shift in charge distribution to the (N-donor)$_2Cu^{II}$(Cat) redox isomer. Four coordinate complexes of Cu(II) are generally square planar, although tetrahedral structures are known, and, in this redox isomer, spin is concentrated on the metal resulting in EPR spectral anisotropy and strong $^{63,65}Cu$ hyperfine coupling [34]. It has been of interest to prepare copper–quinone complexes at the point where metal and quinone orbital energies are balanced so that, shifts in charge distribution may be induced thermally. Structural characterization on d^{10} $(Ph_3P)_2Cu^{I}$(SQ) and d^9 (bpy)Cu^{II}(Cat) complexes indicate

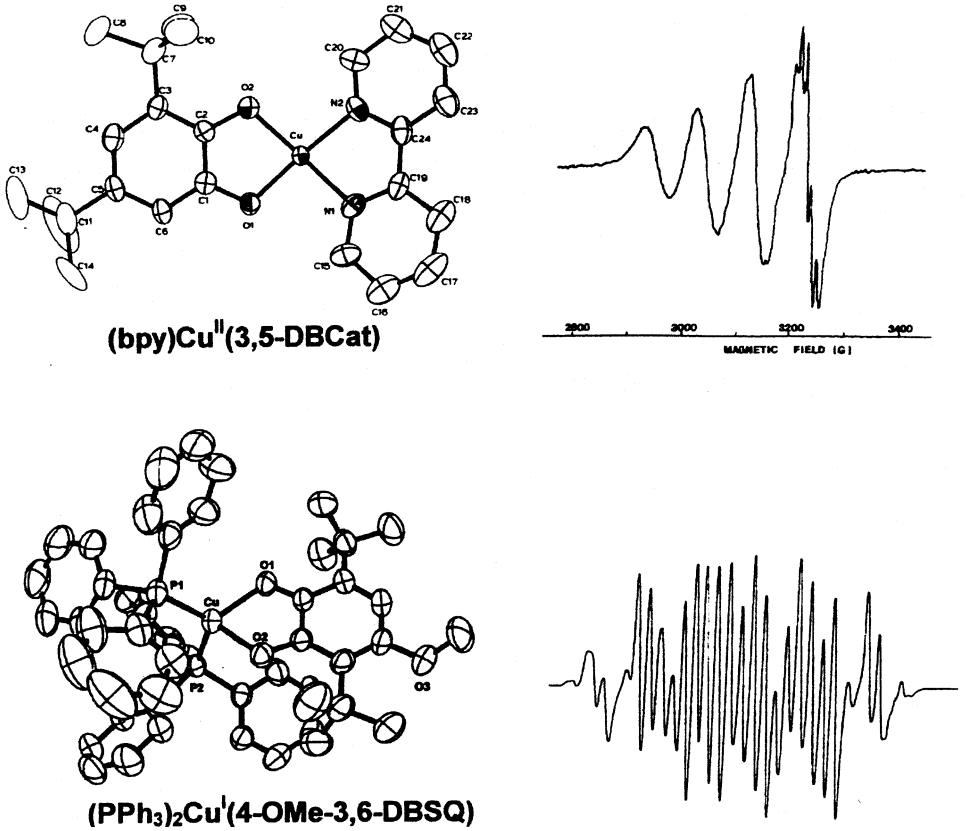

Fig. 23. Changes in structure and EPR spectrum for the L_2Cu^{I}(SQ) and L_2Cu^{II}(Cat) redox isomers of Cu.

that the Cu–O bond length of the Cu(I) isomer is roughly 0.15 Å longer than values observed for Cu(II) redox isomers. Changes in entropy and enthalpy that define *T*c for Co and Mn complexes may result in temperature-dependent equilibria for L_nCu^{II}(Cat) and L_nCu^{I}(SQ) redox isomers. The strong preference of Cu(I) for a tetrahedral geometry and the tendency for Cu(II) to form planar complexes may present a barrier to electron transfer, but the significance of this effect is undetermined. Observations by Dooley and coworkers on EPR spectra for the reduced Cu-topaquinone (TPQ) site of amine oxidase indicated a change in hyperfine coupling that would be consistent with an equilibrium between $Cu^{I}(TPQ^{SQ})$ and $Cu^{II}(TPQ^{Cat})$ species for the reduced and radical semiquinone forms of TPQ [35]. The reduced Cu(I) center provides a site for dioxygen binding in the mechanism for oxidation to the active form of the enzyme.

The viability of an equilibrium between Cu redox isomers has been demonstrated in two recent publications. Abakumov described observations on the solvent-dependent EPR spectra of a (N-N)Cu(Cat) complex prepared with 4-chloro-3,6-di-*tert*-butylcatechol and with di-*tert*-butyl-1,4-diazabutadiene as the ancillary ligand. Changes in EPR spectrum were interpreted as indicating the existence of an equilibrium mixture of redox isomers [36]. However, crystallographic characterization indicated that the complex consisted of separate $[Cu^{I}((t\text{-}BuN)_2C_2H_2)_2]^{+}$ cations and $[Cu^{II}(SQ)(Cat)]^{-}$ anions [37]. In early work we had found that a bidentate phosphorus-nitrogen ligand gave only (P-N)Cu^{I}(3,5-DBSQ) species [41], but, recently, Kaim described temperature-dependent shifts in the EPR spectrum of a copper complex of 3,5-di-*tert*-butylcatechol containing a nitrogen-sulfur coligand [38]. In research with Gabor Speier we have described a copper complex of 9,10-phenanthrenequinone that exhibits equilibrium between redox isomers [39]. This observation is significant not only as an example of VT for a copper-quinone system, but it is the first complex of any metal to show VT for a quinone ligand that is not of the DBBQ family.

Metallic copper reacts with 9,10-phenanthrenequinone (PhenBQ) and pyridine to give $(py)_2Cu(PhenQ)_2$ [40]. Crystallographic characterization has shown that the copper is square pyramidal with pyridine and 9,10-phenanthrenediolate (PhenCat) ligands coordinated in the basal plane (Fig. 24). An unreduced PhenBQ ligand is weakly coordinated through one quinone oxygen at the apical site and paired with the planar PhenCat ligand. Optical spectra indicate that the benzoquinone ligand dissociates in solution, and EPR spectra recorded on solid samples of $(py)_2Cu^{II}$(PhenCat)(PhenBQ) are typical of Cu(II). EPR spectra recorded on the complex in solution show dependence upon both solvent and temperature. In pyridine solution, spectral changes show the existence of an equilibrium between Cu^{II}(Cat) and Cu^{I}(SQ) species with a clear shift in the magnitude of copper hyperfine coupling with the shift in paramagnetic center from the metal to ligand at higher temperatures (Fig. 25). As toluene is added to a pyridine solution the temperature range of the equilibrium drops, and in 10:1 toluene/pyridine glass the equilibrium appears with a transition temperature just above 77 K (Fig. 26). Since there is little mobility in the glass, copper-quinone ET occurs intramolecularly for the equilibrium between $(py)_2Cu^{II}$(PhenCat) and $(py)_2Cu^{I}$(PhenSQ) redox isomers.

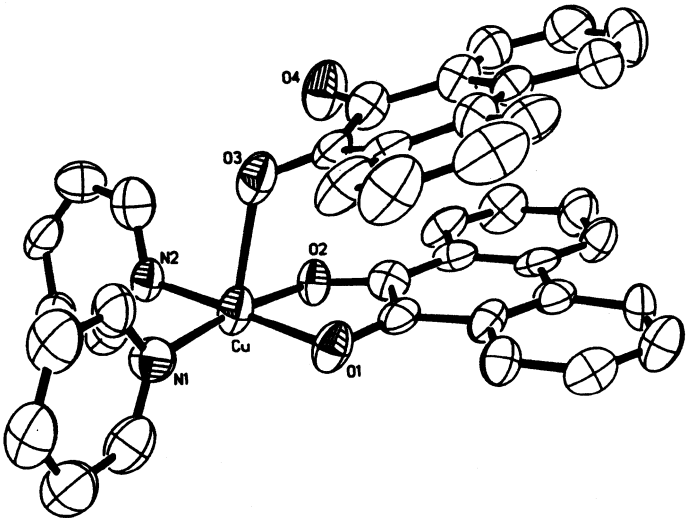

Fig. 24. View of $(py)_2Cu^{II}(PhenCat)(PhenBQ)$.

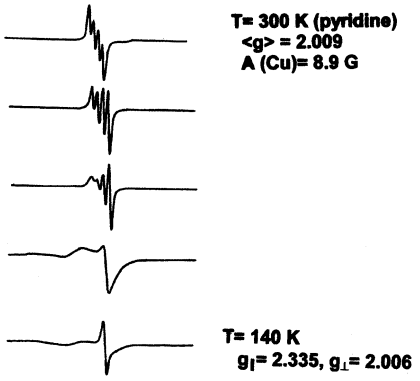

Fig. 25. Temperature-dependent changes in the EPR spectrum of $(py)_2Cu^{I}(PhenSQ)$ with the shift to $(py)_2Cu^{II}(PhenCat)$ in pyridine solution.

5. Conclusions

The conditions that lead to valence tautomerism are clear. Metal and quinone electronic levels must lie close in energy and remain localized in the electronic structure of the complex. Often orbital match is the fortuitous result of coligand donation and quinone substituent effects. Orbital integrity is required to produce the ligand field energy changes that define $\Delta H°$, $\Delta S°$, and Tc for equilibrium. Complexes of the second and third row metals, and particularly the $Ru(N\text{-}N)(Q)_2$ series, show the effects of chelate-ring delocalization that eliminate the possibility of VT for complexes of the larger metals. Ligand field effects must include a large

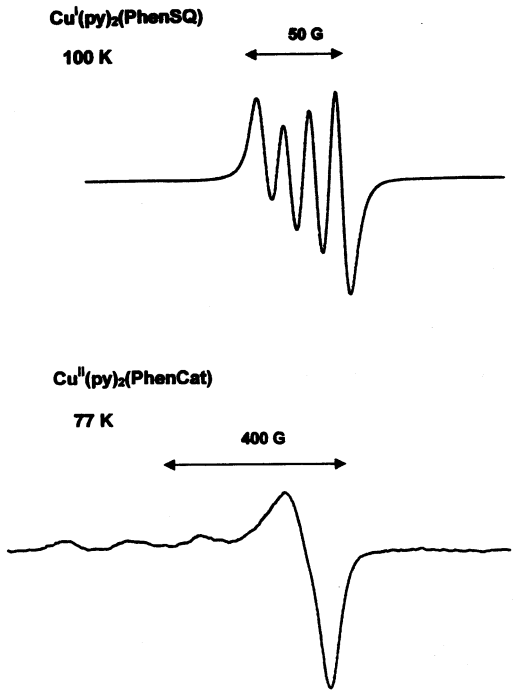

Fig. 26. Changes in the EPR spectrum of $(py)_2Cu^{I}$(PhenSQ) with the shift to $(py)_2Cu^{II}$(PhenCat) in a 10:1 toluene/pyridine glass.

positive entropy change for equilibria that are strongly temperature-dependent, and a large positive enthalpy change to offset the entropy change at *T*c. The examples described in this review are all complexes that exist in a rigid tightly bound isomer that converts to a loose, fluctional product upon electron transfer. Other metal–quinone combinations may potentially exhibit VT. The Cr^{III}(Cat) | Cr^{II}(SQ) couple has many of the properties of the Co and Mn complexes. Bimetallic complexes that undergo changes in metal–metal bonding with shifts in charge distribution may show temperature-dependent equilibria between redox isomers. Potential applications for systems that exhibit VT have been considered in other reviews and extend from switches and sensors to cofactor function in metalloenzymes. Studies on this aspect of the project offer the greatest challenges, and, potentially, the highest rewards.

Acknowledgements

It is a pleasure to recognize the contributions of the scientists who carried out this research at the University of Colorado. Initial observations on VT for complexes of cobalt were made by Dr Robert Buchanan. This research was

developed further by Dr Ok-Sang Jung and, later, with his research group at the Korea Institute for Science and Technology. Studies on complexes of manganese and iron were carried out by Dr Attia Attia. Studies on VT for complexes of copper were carried out collaboratively with Professor Gabor Speier and his group at Veszprem University and by Dr Anne Whalen at the University of Colorado. Our thanks to Professor David Shultz for providing a copy of his review prior to publication.

References

[1] C.G. Pierpont, R.M. Buchanan, Coord. Chem. Rev. 38 (1981) 45.
[2] C.G. Pierpont, C.W. Lange, Prog. Inorg. Chem. 41 (1994) 331.
[3] F. Röhrscheid, A.L. Balch, R.H. Holm, Inorg. Chem. 5 (1966) 1542.
[4] (a) A. Dei, D. Gatteschi, Inorg. Chim. Acta 198 (1992) 831. (b) C.W. Lange, B.J. Conklin, C.G. Pierpont, Inorg. Chem. 33 (1994) 1276.
[5] R.M. Buchanan, C.G. Pierpont, J. Am. Chem. Soc. 102 (1980) 4951.
[6] P. Chaudhuri, M. Hess, K. Hildenbrand, E. Bill, T. Weyhermüller, K. Wieghardt, Inorg. Chem. 38 (1999) 2781.
[7] D.A. Shultz, in: J.S. Miller, M. Drillon (Eds), Magnetoscience–From Molecules to Materials, Wiley-VCH, New York, in press.
[8] P. Gütlich, A. Dei, Angew. Chem. Int. Ed. Engl. 37 (1997) 2734.
[9] Research in progress.
[10] R.M. Buchanan, C.G. Pierpont, Inorg. Chem. 18 (1979) 3439.
[11] D.M. Adams, A. Dei, A.L. Rheingold, D.N. Hendrickson, J. Am. Chem. Soc. 115 (1993) 8221.
[12] O.-S. Jung, C.G. Pierpont, Inorg. Chem. 33 (1994) 2227.
[13] C.G. Pierpont, O.-S. Jung, Inorg. Chem. 34 (1995) 4281.
[14] D.M. Adams, D.N. Hendrickson, J. Am. Chem. Soc. 118 (1996) 11515.
[15] O.-S. Jung, D.H. Jo, Y.-A Lee, Y.S. Sohn, C.G. Pierpont, Inorg. Chem. 37 (1998) 5875.
[16] A.S. Attia, O.-S. Jung, C.G. Pierpont, Inorg. Chim. Acta 226 (1994) 91.
[17] D.M. Adams, L. Noodleman, D.N. Hendrickson, Inorg. Chem. 36 (1997) 3966.
[18] O.-S. Jung, C.G. Pierpont, J. Am. Chem. Soc. 116 (1994) 2229.
[19] G.A. Abakumov, V.K. Cherkasov, M.P. Bubnov, O.G. Ellert, Z.B. Dobrokhotova, L.N. Zakharov, Y.T. Struchkov, Dokl. Akad. Nauk 328 (1993) 12.
[20] C.W. Lange, M. Földeaki, V.I. Nevodchikov, V.K. Cherkasov, G.A. Abakumov, C.G. Pierpont, J. Am. Chem. Soc. 114 (1992) 4220.
[21] O.-S. Jung, D.H. Jo, Y.-A Lee, B.J. Conklin, C.G. Pierpont, Inorg. Chem. 36 (1997) 19.
[22] D. Ruiz, J. Yoo, I.A. Guzei, A.L. Rheingold, D.N. Hendrickson, Chem. Commun. (1998) 2089.
[23] A. Caneschi, A. Cornia, A. Dei, Inorg. Chem. 37 (1998) 3419.
[24] S.K. Larsen, C.G. Pierpont, J. Am. Chem. Soc. 110 (1988) 1827.
[25] G. Speier, J. Csihony, A.M. Whalen, C.G. Pierpont, Inorg. Chem. 35 (1996) 3519.
[26] K.D. Magers, C.G. Smith, D.T. Sawyer, Inorg. Chem. 19 (1980) 492.
[27] M.W. Lynch, D.N. Hendrickson, B.J. Fitzgerald, C.G. Pierpont, J. Am. Chem. Soc. 103 (1981) 3961.
[28] M.W. Lynch, D.N. Hendrickson, B.J. Fitzgerald, C.G. Pierpont, J. Am. Chem. Soc. 106 (1984) 2041.
[29] A.S. Attia, C.G. Pierpont, Inorg. Chem. 34 (1995) 1172.
[30] A.S. Attia, C.G. Pierpont, Inorg. Chem. 36 (1997) 6184.
[31] A.S. Attia, C.G. Pierpont, Inorg. Chem. 37 (1998) 3051.
[32] A. Caneschi, A. Dei, Angew. Chem. Int. Ed. Engl. 37 (1998) 3005.
[33] A.S. Attia, S. Bhattacharya, C.G. Pierpont, Inorg. Chem. 34 (1995) 4427.

[34] G. Speier, S. Tisza, Z. Tyeklar, C.W. Lange, C.G. Pierpont, Inorg. Chem. 33 (1994) 2041.
[35] K. Warncke, G.T. Babcock, D.M. Dooley, M.A. McGuirl, J. McCracken, J. Am. Chem. Soc. 116 (1994) 4028.
[36] G.A. Abakumov, V.A. Garnov, V.I. Nevodchikov, V.K. Cherkasov, Dokl. Akad. Nauk SSSR 304 (1989) 107.
[37] L.N. Zakharov, Y.N. Saf'yanov, Y.T. Struchkov, G.A. Abakumov, V.K. Cherkasov, V.A. Garnov, Koord. Khim. 16 (1990) 802.
[38] J. Rall, M. Wanner, M. Albrecht, F.M. Hornung, W. Kaim, Chem. Eur. J. 5 (1999) 2802.
[39] G. Speier, Z. Tykelar, L. Szabo, P. Toth II, C.G. Pierpont, D.N. Hendrickson, in: H.D. Barton, A.E. Martell, D.T. Sawyer (Eds.), The Activation of Dioxygen and Homogeneous Catalytic Oxidation, Plenum Press, New York, 1993, p. 423.
[40] Manuscript in preparation.
[41] R.M. Buchanan, C. Wilson-Blumenberg, C. Trapp, S.K. Larsen, D.L. Green, C.G. Pierpont, Inorg. Chem. 25 (1986) 3070.